

Channel Opening Motion of $\alpha 7$ Nicotinic Acetylcholine Receptor as Suggested by Normal Mode Analysis

Xiaolin Cheng^{2,4*}, Benzhuo Lu^{1,2}, Barry Grant^{1,2}, Richard J. Law^{2,4,5}
and J. Andrew McCammon^{1,2,3,4}

¹Department of Chemistry and Biochemistry, University of California at San Diego, La Jolla CA 92093-0365, USA

²Center for Theoretical Biological Physics, University of California at San Diego, La Jolla, CA 92093-0365, USA

³Department of Pharmacology University of California at San Diego, La Jolla, CA 92093-0365 USA

⁴Howard Hughes Medical Institute, University of California at San Diego, La Jolla, CA 92093-0365, USA

⁵Biosciences Division, Lawrence Livermore National Labs 7000 East Avenue, Livermore CA 94550, USA

The gating motion of the human nicotinic acetylcholine receptor (nAChR) $\alpha 7$ was investigated with normal mode analysis (NMA) of two homology models. The first model, referred to as model I, was built from both the *Lymnaea stagnalis* acetylcholine binding protein (AChBP) and the transmembrane (TM) domain of the *Torpedo marmorata* nAChR. The second model, referred to as model C, was based solely on the recent electron microscopy structure of the *T. marmorata* nAChR. Despite structural differences, both models exhibit nearly identical patterns of flexibility and correlated motions. In addition, both models show a similar global twisting motion that may represent channel gating. The similar results obtained for the two models indicate that NMA is most sensitive to the contact topology of the structure rather than its finer detail. The major difference between the low-frequency motions sampled for the two models is that a symmetrical pore-breathing motion, favoring channel opening, is present as the second most dominant motion in model I, whilst largely absent from model C. The absence of this mode in model C can be attributed to its less symmetrical architecture. Finally, as a further goal of the present study, an approximate open channel model, consistent with many experimental findings, has been produced.

© 2005 Elsevier Ltd. All rights reserved.

Keywords: acetylcholine receptor; ion channel; normal mode analysis; allosteric mechanism

*Corresponding author

Introduction

The nicotinic acetylcholine receptor (nAChR) is a ligand-gated ion channel responsible for fast signal transduction across different synapses.^{1–3} The channel is opened transiently in response to the binding of neurotransmitter molecules such as acetylcholine. Structurally, nAChR is composed of a pentameric assembly of five homologous membrane-spanning subunits oriented around a central pore. Each of the subunits is composed of an

extracellular (EC) ligand-binding domain and four transmembrane (TM) helical segments M1–M4, the second of which, M2, forms the channel lumen. Each EC domain contains a core of ten β -strands arranged as a curled β -sandwich. Strands $\beta 1$ to $\beta 6$ form an inner sheet, while strands $\beta 7$ to $\beta 10$ form a second outer sheet. A signature Cys loop, located towards the bottom of the EC domain, joins the inner and outer sheets. The acetylcholine-binding sites lie at the subunit interfaces, and are formed mainly by residues from loops A, B and C of one subunit (the principal side) and loops D, E and F of the other (the complementary side).

Earlier kinetic studies established that nAChR can exist in at least three conformations with different functional properties: closed, open and desensitized.^{4,5} However, molecular details remained somewhat elusive until the crystallographic structure of an acetylcholine binding protein (AChBP) from *Lymnaea stagnalis* became

Abbreviations used: nAChR, nicotinic acetylcholine receptor; AChBP, acetylcholine binding protein; EC, extracellular; TM, transmembrane; MD, molecular dynamics; NMA, normal mode analysis; RTB, rotational-translational block; RMSF, root-mean-square fluctuation; RMSD, root-mean-square deviation.

E-mail address of the corresponding author: xcheng@mccammon.ucsd.edu

available.⁶ This water-soluble homolog of the nAChR EC domain serves as a useful high-resolution structural model for the nAChR ligand-binding domain. A number of crystal structures of AChBPs complexed with different ligands such as *N*-2-hydroxyethylpiperazine-*N'*-2-ethanesulfonate acid (Hepes⁶), agonist (nicotine, carbamoylcholine⁷) and antagonist (α -cobratoxin,⁸ α -conotoxin⁹) have now been solved. From a comparison of these structures it seems that only loops C and F undergo significant conformational change with the presence of different ligands and that the relative orientation of the subunits, within the pentamer, remains unchanged. However, how these structural changes, observed in AChBPs, relate to those in nAChRs during the gating process is currently unclear. Recently, the structure of nAChR from *Torpedo marmorata* was determined by electron microscopy to a resolution of 4 Å.¹⁰ This refined structure provides a detailed model of both the EC and the TM domains of the receptor in a closed state. Further, by fitting the Hepes-bound AChBP structure into the electron density of *Torpedo* nAChR, Unwin *et al.* were able to suggest how the EC domain might respond to agonist binding. Together with evidence for the rotation of the M2 helix during gating, as indicated by earlier low-resolution electron microscopy data¹¹ and later supported by disulphide bond trapping experiments,¹² Unwin *et al.* proposed a model for the gating mechanism, in which the acetylcholine-triggered rotations in the EC domains of α subunits are transmitted to the pore gate through the M2 helices.

Although the general framework governing the gating mechanism provided by the recent electron microscopy experiments has been very satisfactory in integrating a large body of structural data obtained by techniques such as mutagenesis,^{13,14} photo-labeling¹⁵ and fluorescence,¹⁶ the detailed dynamics of the transition, including the essential interactions involved, has not been determined, partly due to the unavailability of a high-resolution open channel structure. Molecular dynamics (MD) simulations have proven to be useful in piecing together the data collected from various sources and bridging the gap between two or more static structures.^{17,18} Previous MD studies of the EC domain of the $\alpha 7$ nAChR revealed that the binding of agonist induces a symmetrical expansion of the five subunits, whereas a more closed and asymmetrical arrangement was seen for the apo and antagonist binding.¹⁹ More recently, a twist-to-close motion that correlates movements of the C-loop with the 10° rotation and inward movement of the subunits A and D was observed in a 15 ns simulation of the $\alpha 7$ receptor.²⁰

Despite having many successful applications, conventional MD simulations are generally limited to submicrosecond time periods. This makes it difficult to explore directly conformational changes with significant kinetic barriers, such as the gating transitions of nAChR. Special simulation

techniques such as targeted MD²¹ and steered MD²² have been devised to address this difficulty. In these methods, in addition to the forces derived from potential functions, an external biased force is applied to guide the system toward the desired end structure. It should be noted that by removing the artificial forces using the weighted-histogram method²³ or Jarzynski's equality,²⁴ the equilibrium thermodynamic and kinetic quantities such as the potential of mean force and the transition rate can be estimated from these biased simulations.

A major goal of our research on the human $\alpha 7$ nAChR is to carry out advanced MD simulations to characterize the detailed dynamics during channel gating. However, before undertaking such large-scale simulations, it is essential to have an insight into the nature of the transition. It is for this reason that we first performed normal mode analysis (NMA) to examine the intrinsic flexibility of the receptor, and to identify the most probable direction of the gating transition. NMA, which is based on the harmonic approximation of the system, has previously been demonstrated to be useful in studying large-scale motions in supramolecular complexes such as the GroEL chaperonin,²⁵ hemoglobin,²⁶ F₁-ATPase,²⁷ ribosome,²⁸ and others.^{29,30} A recent improvement of NMA³¹ based on the rotational-translational block (RTB) method³² described by Tama *et al.* has allowed it to be used in biomolecular assemblies of ~10,000 residues (conventional NMA is usually limited to systems composed of less than 300 residues). The major assumption behind the RTB is that low-frequency normal modes of proteins can be described as pure rigid-body motions of blocks of consecutive amino acid residues. Because of this simplification, the size of the Hessian matrix is reduced, such that the computational cost associated with its storage and diagonalization are greatly decreased. As the current study focuses on a few low-frequency modes of the $\alpha 7$ receptor, the RTB method seems to be an appropriate choice.

Now we turn to the possible $\alpha 7$ structural models that can be used in the RTB studies. Early on, a homology model (called model I) based on the combination of the AChBP structure and channel pore of *Torpedo* nAChR was constructed and studied with theoretical methods such as elastic network NMA³³ and MD simulations.²⁰ However, there are certain concerns about the accuracy of this model: the interface region between the EC and TM domains is not sufficiently addressed; additionally the AChBP-derived EC domain may represent an activated/desensitized state, whereas the TM domain from the nAChR is in the closed/resting state. Consequently, the merged structure could be mismatched or represent an intermediate structure, provided gating occurs in a step-wise process and structural change in the EC domain precedes the movement of the channel pore.³⁴

The recent 4.0 Å resolution electron microscopy structure of the *Torpedo* nAChR with both the EC and TM domains should provide a better

template for modeling nAChRs.¹⁰ However, complications arise, as *Torpedo* nAChR is a heteropentamer with only two active α subunits. Thus it is not known whether all five subunits of the homopentameric $\alpha 7$ assume the same conformation, or if only two of the subunits are α -like as in the *Torpedo* structure. Here, we have chosen to build a homology model, which will be referred to as model C below, on *Torpedo* nAChR without imposing 5-fold symmetry.

Here, we report the application of the RTB normal mode analysis to the above-mentioned structural models. We compute the root-mean-square fluctuations (RMSF) to examine the overall flexibility of the receptor, and construct cross-correlation maps to identify the interactions that may play a role in mediating the channel gating process. Results indicate that the opening of the channel most likely involves a global twisting motion. Two lines of evidence support this view: first, the majority of results for the I and C models are similar except for some modest differences in a few low-frequency motions; namely, a symmetrical expansion motion that is the second dominant motion in model I is changed considerably in model C. Second, our normal mode results are consistent with a large body of previous experimental data deduced from cysteine accessibility,¹ affinity labeling,³⁵ mutagenesis³⁶ and electron microscopy experiments.¹¹ Moreover, the significant motion of the C-loop regions and the asymmetrical expansions agree well with MD simulations of the $\alpha 7$ EC domain.^{19,37} A similar global twisting motion has also been observed recently both in an elastic

network model³³ and in a MD simulation of the $\alpha 7$ nAChR.²⁰

Results and Discussion

Comparison of two $\alpha 7$ models

The AChBP derived model I has been used in a number of earlier computational studies.^{20,33} With the availability of a second, potentially more accurate, model based on the recent *Torpedo* receptor structure, it is of interest to make a detailed structural comparison of the two models. A superposition of the two structures based on the backbone atoms of their EC domains (residues 20–205) is displayed in Figure 1(a). Overall, the structures were found to be highly similar in their EC domains (with a root-mean-square deviation (RMSD) of 2.7 Å). The major structural differences were found to reside in loops C and F. These two loops are the main components of the principal and complementary faces of the subunit interface. In model C, both loops appear more loosely structured. For example, the tip of the C-loop is slightly dislodged from its conformation close to the ligand-binding site in model I. These alternate loop conformations reflect the differences between the two model template structures.

Additional differences between the models occur in the Cys and $\beta 1$ – $\beta 2$ loops, located at the bottom of the EC domain. Superposition of the structures on the backbone atoms of their TM domains, as shown in Figure 1(b), reveals that the Cys and $\beta 1$ – $\beta 2$ loops

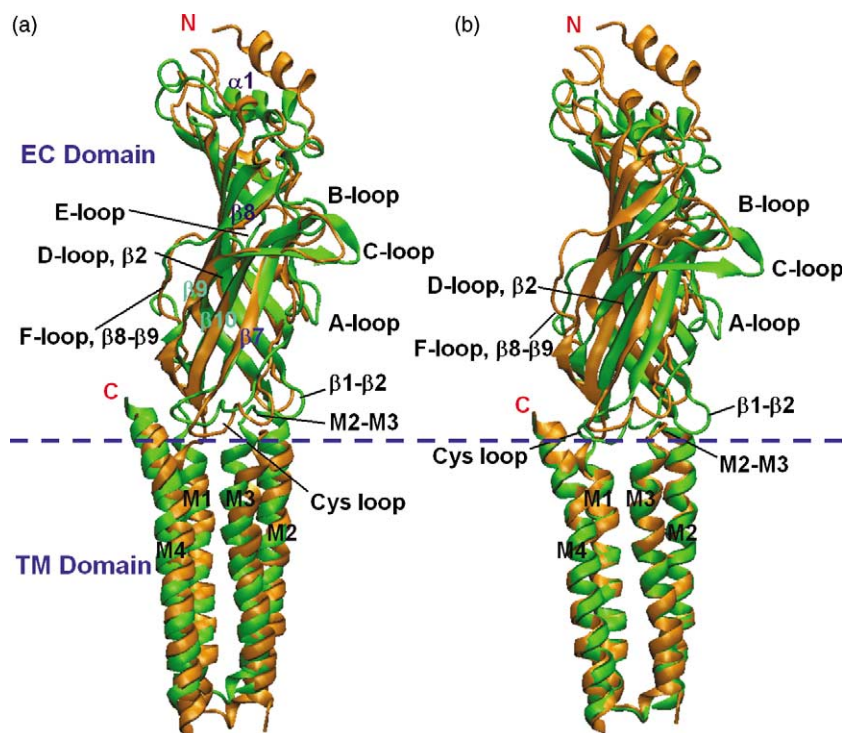


Figure 1. Comparison of α subunits in the C model (in orange) and in the I model (in green), as viewed parallel with the membrane plane from the periphery of the channel. The blue broken line divides the subunit into two parts, the EC domain and the TM domain. (a) Superposition on the EC domain except the $\alpha 1$ helix. (b) Superposition on the TM domain.

are not in equivalent locations relative to the M2–M3 linkers. Relative to model C, the loops are markedly displaced, bringing the Cys loop (1–2 Å) and the β 1– β 2 loop (3–4 Å) closer to the M2–M3 linker.

In conclusion, the major structural elements of model I should be considered as reasonably accurate. This extends to the Cys loop (with an RMSD of 2.7 Å between two models) despite the low sequence identity of α 7 and AChBP. However, differences between the models in the positioning of the EC and TM domains may indicate an error in model I or may be an outcome of ligand-binding. Differences are particularly evident in the β 1– β 2 region, which is shifted away from the membrane surface by 3–4 Å in model C. Regardless of the origin of these differences, it is interesting to examine how their different interactions might affect the dynamics of the receptor. The following sections detail the results of RTB analysis of both models, in which each residue is considered as a block.

Root-mean-square fluctuations (RMSF)

Figure 2 illustrates the RMSFs for models I (red line) and C (green line) along with the experimental data derived from B -factors for AChBP (black line). Residue equivalences between the EC domain of the α 7 and AChBP are as denoted by Henchman *et al.*³⁷ For clarity, only the average RMSFs for all five subunits are shown. The fluctuation profile for both models is very similar (correlation coefficient of 0.96). Despite differences in the Cys and β 1– β 2 loops, the overall flexibility of the whole receptor does not seem to depend on the finer structural details of this region and indicates that both models have a level of accuracy suitable for coarse-grained NMA studies.

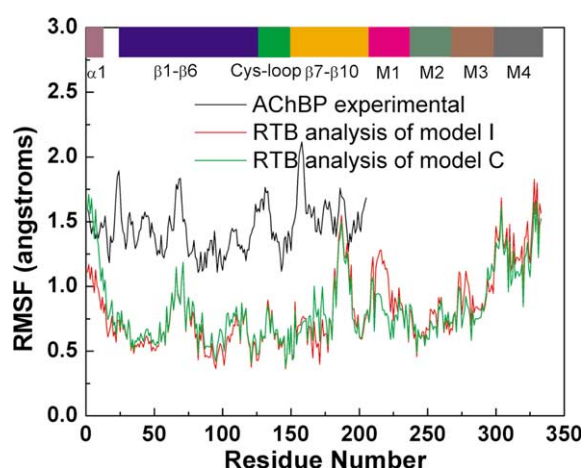


Figure 2. The RMSFs of the C^α atoms at 300 K for the C model (green line) and the I model (red line) calculated from the RTB normal mode analysis, as compared to the experimental data (black line) of the equivalent region of the AChBP. The experimental RMSFs were calculated from the B -factors of the AChBP (PDB code: 119B) using $\text{RMSF} = \sqrt{(3/8\pi^2)B_{\text{factor}}}$. For clarity, the RMSFs are averaged over five subunits.

The magnitude of B -factor-derived data was found to be much larger than those obtained from RTB calculations. It should be noted, however, that the fluctuation pattern is more relevant than the absolute thermal amplitude and, in this sense, a reasonable agreement is evident (correlation coefficient of 0.64). With NMA, it has been demonstrated that although fairly robust results can be obtained for the fluctuation pattern, the magnitude of fluctuation is very sensitive to the energy function and solvation model employed.³⁸

Differences between AChBP B -factors and simulation results are most pronounced in the vicinity of the C-loop (residues 180–197). This region was found to fluctuate significantly about its initial position in simulations of both models. However, as agonist interactions help to stabilize the C-loop in the AChBP structure, it is not surprising to see such differences, since the simulations were performed in the absence of ligand. This result is consistent with previous experimental studies that indicate that the C-loop is flexible when the ligand is not present.³⁹ A similar observation has also been obtained in a recent simulation of the α 7 receptor including a membrane bilayer model.²⁰ Another region that was found to display slight differences was the N terminus, which has a short α -helical structure. RTB calculations on both models indicated a greater mobility in this region than the experimental B -factor data implied. The origin of this difference remains unclear, but may be due to crystal contacts restricting movement of this region in the AChBP structure. The final difference of note occurs around residues 158–160 (in F-loop), which move significantly in AChBP relative to the same region in α 7 nAChR. We find that Gln160 forms two over-stabilized salt-bridges with Phe32 and Ser33 in our calculations, causing the decreased mobility for α 7 nAChR.

In the TM domain, helices M1, M2 and M3 are mostly responsible for the inter-subunit contacts, whilst the M4 helix constitutes the outer layer of the channel. In our RTB calculation, the M4 helix (residues 299–333) exhibits the greatest mobility, which involves a rotation and an outward translation. Although this greater flexibility could be explained by the lack of lipid bilayer in our model, the recent electron microscopy structure of the *Torpedo* nAChR shows helix M4 to be less precisely positioned than the other helices (individual subunits are aligned by positioning them into a strict 5-fold register) suggesting that M4 is indeed more flexible.¹⁰

As expected, most secondary structure elements, such as β strands in the EC domain, exhibit low flexibility (Figure 2). In addition, four loops also show minimal displacements, namely residues 45–50 (β 1– β 2 loop), 92–96 (A-loop, which makes close contacts with the binding site), 120–124 (centered at Cys121 in Cys loop) and 145–150 (centered at Cys147 in Cys loop). This is in agreement with previous MD simulations, which indicated that of the six loops shaping the ligand-binding site, loops A and D are

the mostly rigid, whereas loops B, C and F ($\beta 8$ – $\beta 9$) appear more flexible.³⁷ The rigidity of the $\beta 1$ – $\beta 2$ and Cys loops is consistent with previous experimental results^{2,5} and may be important in transmitting the EC domain motion to the TM domain.

Cross-correlation maps

Central in understanding the allosteric gating mechanism of nAChRs is a description of how structural changes induced at the ligand-binding site are propagated over large distances (~ 45 Å) resulting in the modulation of channel opening events. What are the key residue interactions involved in this structural transmission? Since this question is dynamic in nature, even if two end state crystal structures (in the closed and open conformations) are available, there is still a degree of uncertainty about how the conformational change occurs. In previous applications of NMA, the examination of cross-correlation maps has provided important insight into how a local residue fluctuation correlates with the movement of another distant residue.²⁶

The correlation maps for one subunit are shown in Figure 3. Similar intra-subunit correlation maps were observed for both models (Figure 3(a) and (b)). Figure 3(c) illustrates the inter-subunit correlation for model I, the results for the C model being almost indistinguishable (data not shown). The similar results obtained for two models again lend support to the appropriateness of using low-resolution

homology models in NMA studies. In the following sections, discussion is restricted to results obtained for model I, which are highly similar to those obtained for model C.

As shown in Figure 3(a) and (c), residues within each subunit were found to exhibit cooperative motions, whereas residues in adjacent subunits were relatively uncorrelated, the exception being several residues located at subunit interfaces, such as Asp24 (in $\alpha 1$ – $\beta 1$), Asn46 (in $\beta 1$ – $\beta 2$), Asp96 (in loop A), Leu247 and Cys300 (both residing in the M2 and M4 helices) (see also Figure 3(d)).

In the intra-subunit map (Figure 3(a)), yellow lines divide the map into two regions: the EC domain (bottom left, where the correlation is particularly strong, probably arising from its more compact structure), and TM helices (upper right). Dynamic coupling of these regions stems largely from residues 270–274 (the M2–M3 linker), which are coupled to both residues 43–45 ($\beta 1$ – $\beta 2$ loop) and residues 133–135 (Cys loop) (red box in Figure 3(a)). Although the high level of sequence conservation of the Cys loop suggests that it might play an important role in channel gating, Unwin *et al.* propose that the $\beta 1$ – $\beta 2$ region functions as an actuator, acting on the M2–M3 linker.⁴⁰ A recent experiment with the GABA_A receptor has indicated an alternative possibility; namely, that the $\beta 1$ – $\beta 2$ and Cys loops might act together to coordinate the communication between the ligand-binding domain and TM helices.³⁶ The current correlation analysis seems to favor this last proposal, indicating

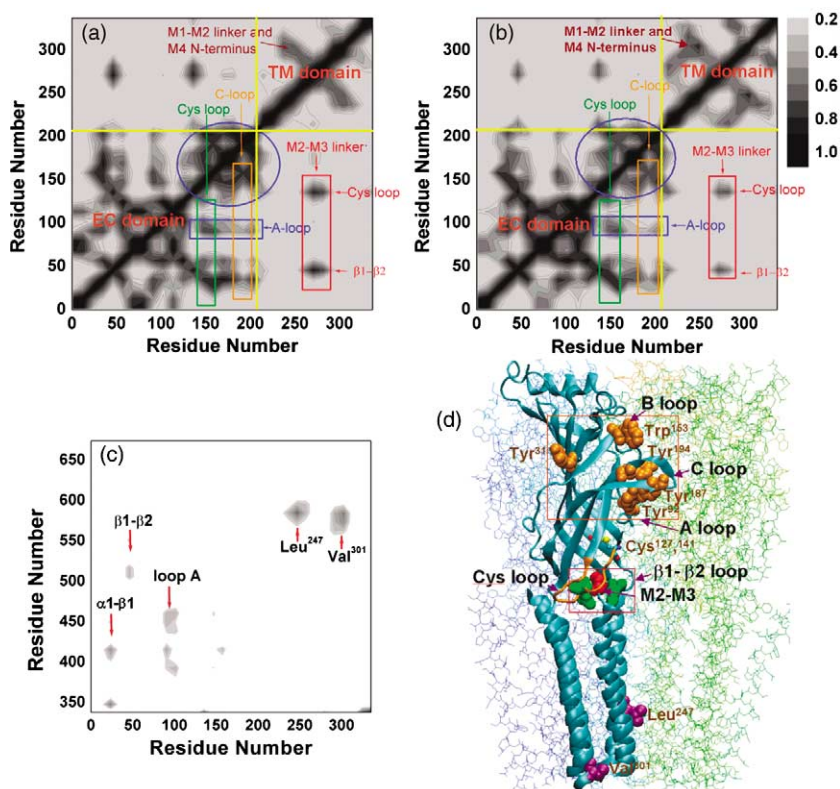


Figure 3. The correlated fluctuations of the C α atoms in the $\alpha 7$ receptor calculated from the RTB analysis. The correlation maps are shown in (a) the intra-subunit correlations in the I model, (b) the intra-subunit correlations in the C model, (c) the correlations between the adjacent subunits in the C/I model. The grey level indicates the strength of the correlation. (d) Structural model of the $\alpha 7$ nAChR with one of the subunits shown in the ribbon representation. Two highly correlated clusters of residues are marked with red boxes, one of which is close to the acetylcholine binding site shown as orange van der Waals spheres (see also the orange box in (a) and (b)). The other is in the M2–M3 linker region shown as green and red van der Waals spheres (see also the red box in (a) and (b)). Two purple van der Waals spheres located in the TM helices denote Leu247 and Val301, which are also indicated in (c), showing notable correlated motions with the residues in other subunits. Also labeled are the locations of the $\beta 1$ – $\beta 2$ loop, the M2–M3 linker and the A, B, C and Cys loops.

that both the Cys and $\beta 1$ – $\beta 2$ loops undergo highly concerted movements with the M2–M3 linker.

The EC domain can be further divided into two subdomains (Figure 3(a)). The first corresponds to residues 127–205 or strands $\beta 7$ – $\beta 10$ (encircled by a blue ellipse), with the second region encompassing residues 1–127 or strands $\beta 1$ – $\beta 6$. Each subdomain essentially undergoes an independent movement as implicated by a clear separation between these two blocks. We note that strands $\beta 1$ – $\beta 6$ form the inner part of the EC domain and have been described by Unwin to undergo a $\sim 10^\circ$ rigid-body rotation relative to the outer sheets upon agonist binding.¹⁰ The correlated motions observed here are therefore consistent with Unwin's observation. The independent motion of the inner EC domain β -strands was found to be one of the most dominant global motions of an isolated subunit and will be discussed in more detail below.

Recently, combined MD simulation and tryptophan fluorescence studies³⁹ have demonstrated that the allosteric effect of agonist binding was initiated from the inward motion of the C-loop. However, a full understanding of how this local conformational change propagates to the pore domain remains to be established. In an effort to shed some light on this issue, we examined the correlated motions of ligand-binding site residues. As highlighted in the orange box in Figure 3(a), Tyr194 and Tyr187 in the C-loop are highly correlated to Tyr92 in the A-loop and Trp153 in the B-loop (orange spheres in Figure 3(d)).

This cluster of residues has been confirmed by experiments to form the principal side of the acetylcholine-binding site.^{6,7} In effect, the concerted movement of these residues facilitates the precise positioning of the ligand. Also evident is the coupling of the Cys loop with the A-loop (residues 92–96) and with the D-loop ($\beta 2$, residues 53–56) (green box in Figure 3(a)). As noted previously, at the membrane interface the Cys loop and the M2–M3 linker are highly correlated, where together with the $\beta 1$ – $\beta 2$ loop they form another strongly related cluster of residues (green and red spheres in Figure 3(d)). Taken together with earlier findings, the current correlation analysis is suggestive of a rough sequential picture for the ligand-gated process. That is, agonist binding first induces an inward motion of the C-loop, which is then transmitted to the Cys loop *via* structural rearrangements around the binding site, such as A, D-loop movement. Finally, channel gating results from the interactions of the Cys loop and $\beta 1$ – $\beta 2$ region on either side of the M2–M3 linker.

Normal modes of an isolated α subunit

Unwin *et al.* have proposed that rotation of the inner β sheets of the EC domain initiates TM pore opening.⁴¹ The rotation within the EC domain was determined from a rigid-body fitting of the Hepes-bound AChBP structure to the electron density map of the closed acetylcholine receptor. However, such

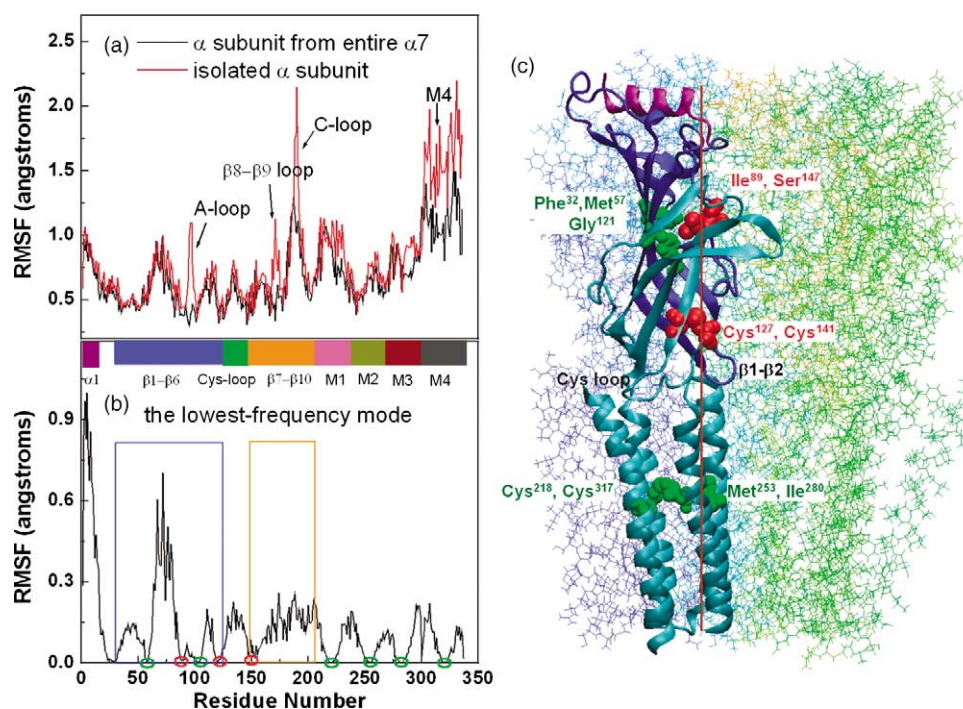


Figure 4. The RTB normal mode analysis of an isolated α subunit. (a) The RMSFs of the C^α atoms (red line) as compared to those from the entire receptor calculation (black line). (b) The RMSFs of the C^α atoms calculated from the lowest frequency mode. The regions of minimum displacements are marked with red or green circles. The color bar in the middle indicates important secondary structural elements. (c) Schematic diagram of the whole receptor with one of the subunits shown in ribbon representation. The red and green van der Waals spheres correspond to the residues with minimum displacements as circled in (b) using the same color-coding. The vertical line passing through two pairs of red residues is a possible axis around which the rotation within the subunit occurs.

a rotational movement was not observed in the recently reported AChBP structures.^{7–9} In an effort to assess the intrinsic flexibility of the α subunit, we performed an NMA study on an isolated α subunit. Figure 4(a) depicts the RMSFs for the isolated subunit in comparison with results obtained for a single subunit from the full $\alpha 7$ receptor. As expected, the RMSFs of the isolated subunit are of greater magnitude than those observed for the entire receptor, especially in the C-loop, A-loop and $\beta 8$ – $\beta 9$ regions. Residues in these regions maintain contacts with neighboring subunits in the full receptor, which are absent in the isolated subunit. The M4 helices also display greater fluctuations in the isolated subunit. The reason for this difference is not obvious, as the M4 helix makes no direct van der Waals contacts with any other subunits.

The lowest frequency modes of proteins are often very important and potentially related to biological function.^{38,42} The RMSFs for the first mode are displayed in Figure 4(b), indicating large, correlated fluctuations of the inner portion of the EC domain (blue box) relative to the outer portion (orange box). Dynamic domains and possible hinge residues were identified with the aid of the Dyndom program.⁴³ This analysis indicated that the overall motion of the first mode could be described approximately as a rigid-body rotation around the hinge residues Ile89, Ser147, Cys127 and Cys141 (red spheres in Figure 4(c)). These positions correspond to points of minimum displacement in Figure 4(b) (labeled with red circles along the horizontal axis). They form two residue pairs, Ile89–Ser147 and Cys127–Cys141, that

maintain close contact at the interface of the inner and outer regions of the EC domain. These positions are speculated to define an axis of rotation within the EC domain (orange vertical line in Figure 4(c)). The rotation of the inner region around the axis running through the center of the disulfide bridge has been described by Unwin *et al.*,⁴¹ who speculated that the highly conserved Cys127 and Cys141 (red circle in Figure 4(b)) might act as a hinge point. Additionally, we propose that residues Ile89 and Ser147 might function as a second stationary point for the rotation. Both Ile89, which sits on the $\beta 4$ strand, and Ser147, which is located in the B loop, are in close proximity to the ligand-binding pocket and may serve as efficient mediators of rotation-activation once the ligand is loaded.

In addition to the four hinge residues described above, we note several other residues displaying minimal RMSF values (Figure 4(b)). These residues are Phe32, Met57, Gly121, Cys218, Met253, Ile280 and Cys317, which have been marked with green circles in Figure 4(b) and highlighted as green van der Waals spheres in Figure 4(c). All these residues are located at the center of secondary structure elements. The former three residues are in the EC domain while the remaining four are in the TM domain. A closer examination of the TM domain residues reveals that there are some kinks formed in these regions after rotation, particularly in M2 and M3. The kinked structure in the vicinity of Leu247 was observed in the closed structure of the *Torpedo* nAChR. However, the M2 and M3 helices appear to be more kinked after the transition toward the open

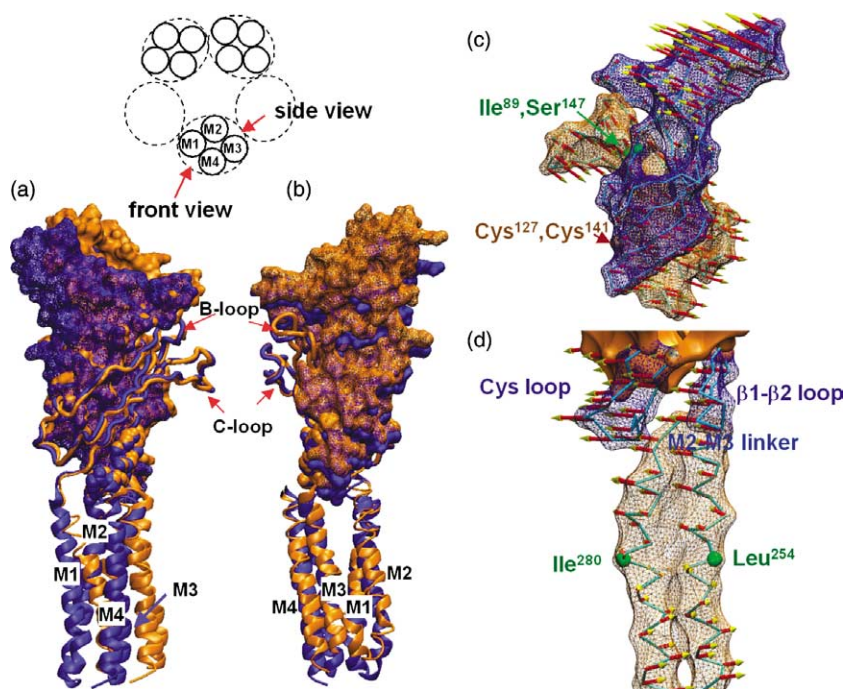


Figure 5. The global motion of a single $\alpha 7$ subunit as suggested by the lowest frequency mode. (a) and (b) Superposition of two structures before (in blue) and after (in brown) a small displacement along the first normal mode. The TM helices are shown as ribbons. The inner set of the EC domain ($\beta 1$ – $\beta 6$) is shown as solid surface representation while the outer set ($\beta 7$ – $\beta 10$) is shown as tubes. A schematic diagram on top of (a) and (b) illustrates the directions of the views. (a) Front view, parallel with the membrane plane. (b) Side view, rotated $\sim 150^\circ$ around the pore axis from (a). (c) and (d) The first mode vectors mapped onto the subunit surface. (c) The EC domain with the inner $\beta 1$ – $\beta 6$ in blue and the outer $\beta 7$ – $\beta 10$ in orange, as viewed parallel with the membrane plane from the inside of the channel. As indicated by the arrows, the motion can be described approximately as a

rotation around the long axis passing through two residue pairs Ile89, Ser147 (green spheres) and Cys127, Cys141 (brown spheres). (d) The EC and TM interface, indicating concerted motions of the $\beta 1$ – $\beta 2$, M2–M3, and Cys loops. Residues Leu254 and Ile280, which have minimal displacements (see also Figure 4(b) and (c)), are shown as green spheres. These residues show some increased tendency to kink during the conformational change as suggested by different movement directions around these regions.

structure (as indicated by the moving direction alteration around residues Leu254 and Ile180, shown as green spheres in Figure 5(d)).

Figure 5(a) and (b) shows a comparison of the two structures before (in blue) and after (in orange) a small rotation along the normal mode direction. The superposition is made based on the backbone atoms of residues in the outer $\beta 7$ – $\beta 10$ strands. The overall movement of the first mode corresponds to the rotation of the inner set of the EC domain (shown as blue and orange filled representation) except the short N-terminal α helix, whereas the outer section remains relatively stationary (shown as blue and orange tubes). The absence of significant structural change in the outer β sheets can be confirmed by the close fitting of residues in this region (RMSD of 1.2 Å on 63 C^α atoms) between two structures. The rotation of the inner part is coupled with motion in the N-terminal region, leading to larger differences at the top of the subunit (Figure 5(a) and (b)). In Figure 5(c), we also show this rotation by mapping the normal mode vector for each C^α onto the mesh surface of the EC domain.

Importantly, the rotation extends from the EC domain to the TM pore region through the interaction of the M2–M3 linker, $\beta 1$ – $\beta 2$ and Cys loops, similar to what has been proposed by Unwin.⁴¹ Using charge mutations in the GABA_A³⁶ and Gly receptors,² several groups have demonstrated the importance of molecular interactions between these three loops in imparting cooperativity in Cys loop receptors. However, due to the limited resolution of the currently available structures, the detailed mechanical role of the $\beta 1$ – $\beta 2$ and Cys loops is still unclear.³ Here, the $\beta 1$ – $\beta 2$, Cys loops and M2–M3 linker appear to rotate in the same direction (Figure 5(d)). But according to the spatial relationship of these three loops, it seems that $\beta 1$ – $\beta 2$ should function as an actuator. This does not exclude the possibility that the Cys loop may act as a stator, bracketing the rotation of the M2–M3 linker when the receptor is activated. The role of the Cys loop as a stator may indicate why the rigidity of the Cys loop is so important. Without the disulphide bond bridging two Cys residues, the 15 residue loop would likely be quite flexible, thus losing its functional role.

Global motion of the entire receptor

In the above RMSF plots and correlation maps, nearly identical results were observed for the two models. Structural differences between the models were found to have a more significant effect on the three primary modes of motion; namely, twisting, symmetrical pore-expansion and asymmetrical pore-expansion. These three types of motion have been identified from model I, each of them corresponding to the first three low-frequency modes, respectively (discussed in detail below). In model C, two major differences were found for these modes. First, the symmetrical pore-expansion motion now becomes the fifth mode, and has a low

correlation (<0.3) with that obtained for model I. The asymmetrical pore-expansion motion becomes the second dominant motion for model C. Second, although the twisting motion remains largely unchanged (correlation ~ 0.6), the modest difference seen at the interface of the EC and TM domains induces a slightly disconcerted motion of $\beta 1$ – $\beta 2$ relative to the M2, M3 helices in model C.

Twisting motion (the first mode in model I)

In both the I and C models, the lowest-frequency mode of the entire receptor involves a global twisting motion of the EC domain relative to the TM domain. The two domains undergo a concerted, opposite-direction rotation around the pore axis. An illustration of this motion is given in Figure 6(a) and (b). Several residues that may act as hinge points for the twisting motion were identified with the aid of the Dyndom program,⁴³ namely, residues 40–51 ($\beta 1$ – $\beta 2$), 170–174 ($\beta 8$ – $\beta 9$ loop), 205–210 ($\beta 10$ –M1 linker) and 258–267 (M2–M3 linker). All of these residues are located at the EC and TM interface, and may be interesting targets for mutagenesis. The motion of all five subunits is very similar, which is also highly related to the rocking-type rotation seen in the isolated subunit. The correlation coefficient for this mode, relative to that in the single subunit, is ~ 0.9 , suggesting that the combination of the five individual motions intrinsic to each subunit leads to the symmetrical closing/opening of the whole channel. Earlier electron microscopy studies have suggested that all five M2 regions undergo a similar gating motion during channel opening.¹¹ A similar motion has also been observed in a computational study using an elastic network model.³³ More recently, an all-atom MD simulation has suggested the occurrence of a twist-to-close motion.²⁰ However, this seemingly opposite result is actually consistent with the current observation, since under the harmonic approximation, a conformational change can occur with the same probability in either direction along a given eigenvector.

In order to assess the functional implication of the identified twisting motion and to determine whether it could possibly contribute to the channel opening process, a model structure was generated by displacing the initial closed structure along the mode vector. Figure 7(b) details the pore radius profile as a function of pore axis for the reconfigured structure. As indicated by the red line in Figure 7(b), the first mode of motion tends to increase the width of the pore in the vicinity of Leu247 and Val251, whereas the pore radius changes little for other parts of the channel. Low-resolution electron microscopy studies of nAChR have also indicated that the channel opens only in the middle of membrane,¹¹ with Leu247 and Val251 acting as two possible gates.⁴⁰ Mutational studies by Labarca *et al.* also indicate that channel gating of nicotinic receptors is governed symmetrically by conserved Leu residues in the M2 domains.³⁵ Both studies add weight to the presently observed

channel open motion, where each of the five Leu247 residues participates independently and symmetrically in a rotation step in the structural transition between the closed and open states.

Although the twisting motion appears to be quite similar in the two $\alpha 7$ models, it is still of interest to examine to what extent these modes are correlated. We therefore compute the correlation between the first mode of model I and the eigenvectors associated with the first 50 modes obtained from model C (Supplementary Data Figure 1S). The first modes from two structures are indeed quantitatively similar, as indicated by the correlation coefficient of ~ 0.6 . The difference between the modes is due to the slightly disconcerted motion seen in the membrane interface in model C. We suspect that the $\beta 1$ – $\beta 2$ and Cys loops, that contact the M2–M3 region, are slightly displaced in the C model, giving rise to the observed differences.

Symmetrical pore-expansion (the second mode in model I)

In contrast to the common twisting motion of the first mode, the motion described by the second mode is different between each of the structures. With model I, the second mode corresponds to a symmetrical pore-expansion of the whole receptor (Figure 6(c)). However, with model C, the second mode corresponds to an asymmetrical expansion (Figure 6(d)). Generally, the eigenvectors obtained for model C show a weaker correlation with the second mode than with the first (Supplementary

Data Figure 1S). We suspect that the decreased symmetrical motion in model C is because the AChBP derived model I is structurally more symmetrical than model C.

As shown in Figure 7(b) (green line), the contribution of the symmetrical pore-expansion motion to channel opening is evident, albeit to a lesser extent than that of the first twisting mode. The pore-breathing motion is also coupled with the stretching/compressing motion along the channel axis (see Supplementary Data). This explains why the green line is dramatically shifted in Figure 7(b). We note that a similar pore-breathing motion of the *Aplysia* AChBP upon agonist binding has been observed recently (P. Taylor, personal communication). An indirect comparison of the apo *Torpedo* nAChR¹⁰ with the liganded AChBP⁶ also indicates a stretching/compressing motion along the channel direction. However, evidence for the latter is not completely convincing, as a more compressed structure could also be attributed to crystal contacts in the AChBP.

Asymmetrical pore-expansion (the third mode in model I)

The asymmetrical pore-expansion motion of the receptor is observed in both models I and C. Consistent with the structural differences between models, this motion is the third lowest mode for model I, whilst it corresponds to the second dominant motion in model C. As shown in Figure 6(d), two subunits, A and D, move outward

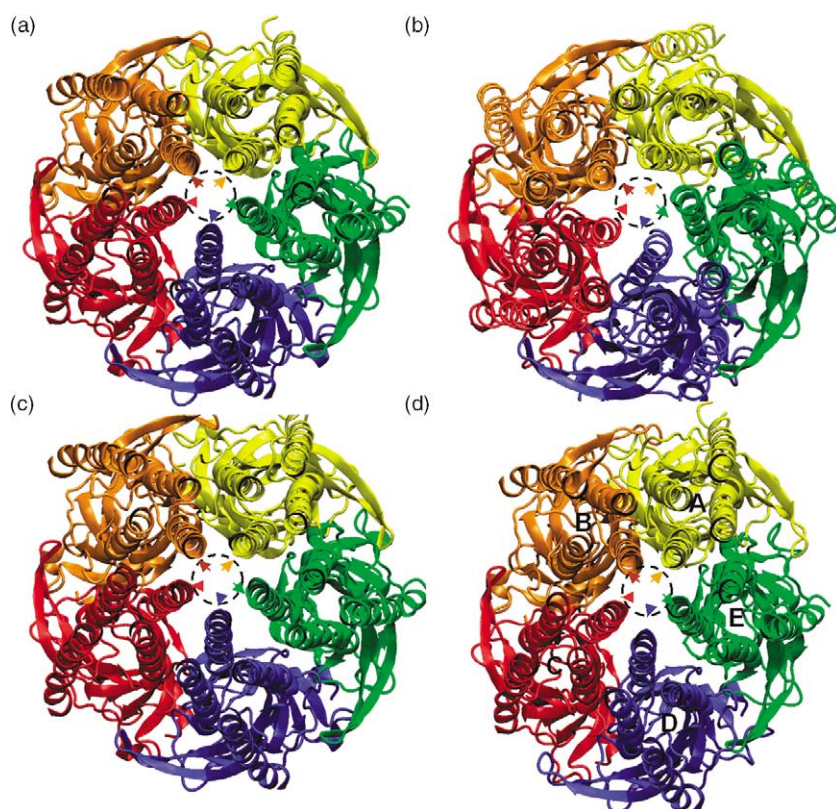


Figure 6. Ribbon diagrams of the $\alpha 7$ receptor, as viewed along the channel axis from the cytoplasm. (a) The starting closed-channel structure. (b)–(d) Model structures generated from a small displacement along the lowest (twisting), the second lowest (symmetrical pore-expansion) and the third lowest (asymmetrical pore-expansion) normal mode vectors of the I model. The broken circles indicate the size of the pore in the closed structure. The five arrowheads point to the corresponding subunits in the closed structure using the same color-coding. These circles and arrowheads help to illustrate the expanding/rotating motions.

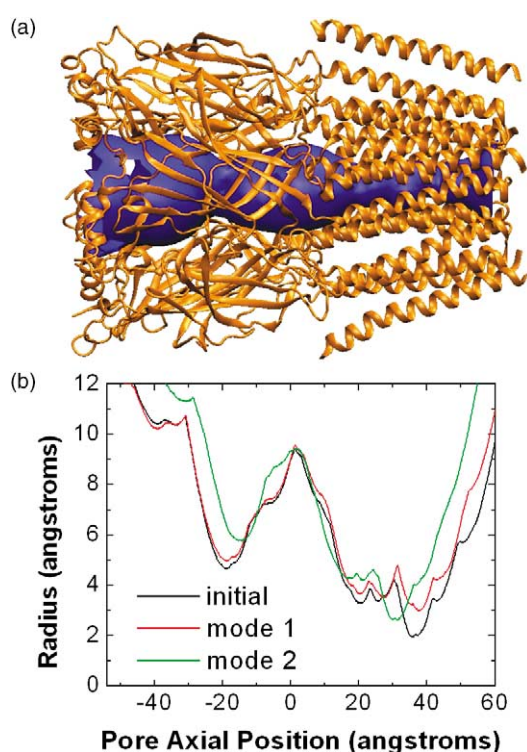


Figure 7. Pore radius profile as a function of the pore axis. Displacements along the first two modes of the I model both tend to increase the minimum pore radius. (a) Cartoon view of the closed structure with the channel pore shown as a blue solid surface representation. The pore radius profile and the solid surface representation are generated using the HOLE program.⁵⁹ (b) Pore radius profiles of two structural models (see also Figure 6(b) and (c)) as compared to that of the closed structure (PDB code: 2BG9). The colors are: the closed, black; mode 1, red; mode 2, green. The shift of the green line is due to the compression of the receptor along the pore axis.

while three other subunits B, C, and E move inward. Such an asymmetric motion has been observed previously in the EC domain and whole receptor simulations.^{20,37} Although an asymmetrical two-site-activation seems to be characteristic for members of the nicotinic receptor family, our results suggest that this manner of motion should not contribute to channel opening (displacement extrapolated from this motion does not result in a wider pore). Moreover, a recent comparison of a low-resolution open structure with a closed channel structure suggested that the pore opened up symmetrically in the middle of the membrane.⁴⁰ Thus, the biological significance of this motion for channel gating remains unclear.

RTB analysis with restraints on the M4 helices

It is well established that the TM domain can be partitioned into two sets of walls: the inner wall (primarily composed of five M2 helices functioning as the channel lumen), and the outer wall

(composed of the remaining M1, M3 and M4 helices that contact the membrane).⁴⁰ Previously it has been suggested that only the inner portion (M2 and possibly part of M1) might move when the receptor is activated.⁴⁰ However, this is in contrast to the large-scale movements of the outer M4 region seen in the current calculations (Figures 2 and 4(a)). We hypothesize that the absence of a membrane environment in the simulation leads to the exaggerated motion of outer wall. The surrounding environment, composed of well-packed lipid molecules, would tend to hinder the movement of the outer wall, whereas the M2 region would still be allowed to move due to its minimal contact with other outer helices. The importance of van der Waals interactions between the lipid bilayer and the M4 segment for allosteric movement of the whole receptor has been recently demonstrated in a 35 ns MD simulation of the *Torpedo* nAChR TM pore.⁴⁴ In addition, mutagenesis experiments of M4 residues as well as the pharmacological role of several ligands that bind in lipid bilayer also seem to support this postulate.^{45,46} To further test this hypothesis, we performed an additional RTB normal mode analysis on model I, in which a harmonic restraint, with a force constant of $3 \text{ kcal mol}^{-1} \text{ \AA}^{-1}$, was applied to each pair of equivalent C^α atoms in the neighboring subunits (Supplementary Data Figure 2S). This simple procedure was designed to mimic the restriction effect of the membrane environment. Remarkably, results indicate that the twisting motion remains as the dominant mode, in which only the interior M2 helices undergo a concerted motion within the EC domain (see Supplementary Data). The survival of the twisting mode in the current restrained RTB analysis confirms that the twist-to-open motion is an intrinsic property of the receptor, and that it is insensitive to the treatment of the bilayer environment.

Proposed open-channel models

Although an atomic-resolution closed-channel structure has emerged recently,¹⁰ the low resolution of the open-channel structure has limited the fitting of secondary structural elements to the electron densities. In an effort to produce an approximate open structure for further study, we sought to perturb the closed structure toward an open conformation along the directions of both the twisting and the symmetrical pore-expansion modes. It should be noted that, although the results from a few low-frequency modes have been successfully used in many previous studies to drive the transition between structures,^{26,47} this type of extrapolation is not always possible. Significant deformation can occur when the energy landscape is complex i.e. the two end states are separated by multiple minima. However, in the recently refined *Torpedo* nAChR structure, it has been shown that the open configuration could be generated from the closed structure through a $\sim 10^\circ$ rotation of the inner β sheets of the EC domain.¹⁰

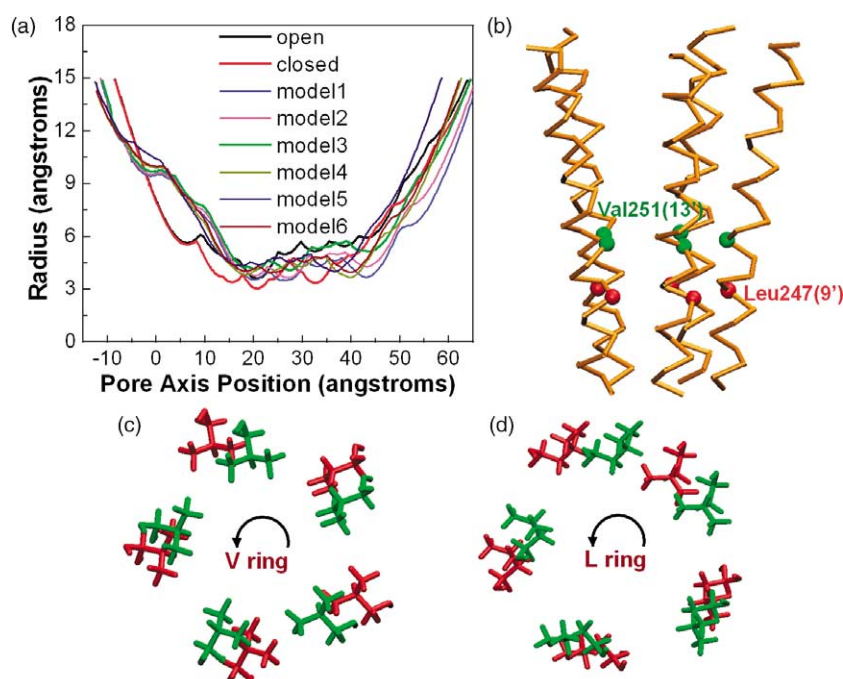


Figure 8. The proposed open-channel models generated by displacing the closed structure along the two lowest frequency modes. (a) Pore radius profiles (pore regions only) of six representative models with backbone RMSD less than 3 Å from the closed structure (model 1, $x=0.8$, $y=150$; model 2, $x=0.8$, $y=100$; model 3, $x=0.9$, $y=150$; model 4, $x=0.9$, $y=100$; model 5, $x=1.0$, $y=150$; model 6, $x=1.0$, $y=100$). These profiles are different from those shown in Figure 7, since the non-polar hydrogen atoms are not added to the models that we show here. The red and black lines correspond to the closed and open structures, respectively, where the closed structure represents a recently refined electron microscopy structure (PDB code: 2BG9) while the open structure coordinates are provided by Unwin based on a low-resolution electron microscopy

image.¹¹ (b) Simplified C α trace representation of the best candidate model for the open channel. Its pore radius profile is the closest match to that of Unwin's open structure. Two elements of the pore gate in the closed channel, the Leu ring (9') and the Val ring (13'), are shown as red and green van der Waals spheres. (c) and (d) The channel is viewed in cross-section. The rotations of Val and Leu rings cause the pore to open up. The structures before and after the rotation are shown as green and red licorice model, respectively.

This relatively small gating motion might therefore justify the extrapolation of normal modes considered here.

Six candidate open structure models were produced using the protocol described in Materials and Methods. Due to the limited resolution of the experimentally determined open structure (TM part only),¹¹ it is not possible to perform direct RMSD-based comparisons with the resulting model structures. As an alternative, pore radius profiles were calculated for the six models (shown in Figure 8(a)) and used to select the most representative structure. In Figure 8(a) the red and black lines correspond to the closed and open structures, respectively. The green line, which corresponds to model 3 (with $x=0.9$, $y=150$, see Materials and Methods), shows the closest similarity to that of the open structure. A trace representation of this model structure is shown in Figure 8(b). The increase of pore radius occurs in the vicinity of two proposed pore gates, namely the Leu ring (9') and the Val ring (13'). We determined that the TM helices, particularly in the L ring and V ring regions (Figure 8(c) and (d)), underwent a clockwise rotation of $\sim 12^\circ$ from the closed structure to produce this putative "open" structure model. It was also noted that a counter-clockwise rotation contributed differently to the pore radius width, creating a more closed structure (data not shown), as occurred in the MD simulation by Law *et al.*²⁰

The current open-channel model indicates that the opening of the channel is caused primarily by rotation of the M2 domains. This finding is in

agreement with Unwin's channel gating model,⁴⁰ and also supported by a recent study, in which a fluorescent group attached near the top of the M2 helix moves into a more hydrophobic environment when the channel opens.⁴⁸ In this open-channel model, the angular rotation of the inner β strands relative to the outer portion of the ligand-binding domain is about 12° , which is similar to the 10° rotation described by Unwin,¹⁰ although there is still a lack of other independent experimental support for this type of rotation. In addition, when moving from the closed-channel nAChR structure toward a putative open-channel model (e.g. model 3), residue Leu212 (equivalent to Val229 in the β subunit of the mouse muscle receptor) is found to change from a buried state to a more water-accessible state, which is consistent with Zhang and Karlin's SCAM experiments⁴⁹ and in agreement with a recent elastic network model calculation.³³

Conclusions

RTB normal mode analysis was used to explore possible mechanisms for the gating motion in the $\alpha 7$ acetylcholine receptor. The two homology models investigated displayed nearly identical RMSFs and cross-correlation patterns. The similarity of results indicates that the earlier and more approximate I model^{20,33} can be used with confidence in coarse-grained normal mode studies. Previous applications of normal mode analysis have shown that the large-scale global motions

captured by the lowest frequency modes are somewhat insensitive to the finer details of structure.²⁷ Consistent with this view, the global twisting motion is similar in both models (correlation coefficient ~ 0.6), whilst less similar results are found for the following modes of motion.

At the tertiary level, the global twisting motion can be described as a synthesis of five similar, rotational movements within each subunit. This rotational motion is an intrinsic property of a single subunit, being present in both monomeric and pentameric forms (correlation coefficient ~ 0.9). Although there is nothing intrinsic in the simulation to induce channel gating (i.e. binding of agonists to the receptor), it is believed that the observed twist-to-open motion may be highly relevant for the gating process, as it is consistent with a number of recent experimental results.^{10,35,40,48,49}

The current simulations also suggest that the $\beta 1$ – $\beta 2$, M2–M3 and Cys loops may play important roles in the gating movement. Cross-correlation analysis indicates that the motions of $\beta 1$ – $\beta 2$, M2–M3 and Cys loop regions are highly correlated. Indeed, the lowest frequency mode obtained for a single subunit corresponds to the concerted motion of these loops. Closer examination suggests that the rotation of TM helices is likely to be driven by the $\beta 1$ – $\beta 2$ loop through its interaction with the M2–M3 linker. The Cys loop, on the other hand, may act as a stator together with $\beta 1$ – $\beta 2$ to bracket the rotation of M2–M3.

In summary, the present study demonstrates that the gating motion deduced experimentally⁴⁰ is plausible from a theoretical perspective, and also provides a putative open-channel model that is consistent with a body of experimental data. Further studies of this open-channel model using non-equilibrium MD methods are currently underway.

Materials and Methods

Homology model building

Two homology models of human $\alpha 7$ receptor were built with Modeller v4.0.^{50,51} The first model, model I, was constructed by combining the 2.7 Å resolution X-ray structure of AChBP⁶ (PDB code: 1I9B) from *L. stagnalis* and the 4.6 Å resolution TM domain of the *Torpedo* nAChR⁴⁰ (PDB code: 1OED). The second model, model C, was built from the recent 4.0 Å resolution electron microscopy structure of *Torpedo* nAChR¹⁰ (PDB code: 2BG9). The homology modeling of model I has been described in detail.²⁰ Briefly, the modeled structure contains 1665 residues comprising both the EC and TM domains but excluding the cytoplasmic vestibule domain between M3 and M4. 5-Fold symmetry was imposed when modeling the pentamer structure. The two templates were joined together by using an overlaid all- α -subunit makeup for the TM domain.

Construction of model C was more straightforward, since a single *Torpedo* nAChR PDB structure was used as the template. The 29 residues in the MA domain were excluded to be consistent with model I. All subunits were modeled simultaneously to help maintain complementarity between subunit interfaces. 5-Fold symmetry was

not imposed, as we did not expect all the subunits to be in the same conformation. Due to either the existence of gaps between the target and template sequences or the low resolution of the template structure, several loop regions required special attention. Missing residues located in the $\beta 7$ – $\beta 8$ loops of the non- α subunits were positioned using coordinates from the α subunits. The $\beta 8$ – $\beta 9$ linkers were modeled based on loops from AChBP. Modeling the C-loop region required extra care. This region is known to be highly variable and can adopt at least three conformations, corresponding to apo, agonist or antagonist occupied. Also, since sequence homology for this region is low between $\alpha 7$ and non- α subunits of *Torpedo* nAChR, models based on non- α templates proved to be unreliable. In the final model, the C-loops in two alternating subunits had the open conformation, according to the α subunits of the *Torpedo* structure, while the remaining subunits had the closed conformation based on AChBP. The final models were evaluated with PROCHECK⁵² and Prosa 2003.⁵³

Rotational-translational block normal mode (RTB)

The application of conventional NMA to large biomolecular systems is limited by the computational cost associated with the storage and diagonalization of all-atom Hessian matrix. The RTB (rotations-translations of blocks) method, proposed by Tama *et al.*, employs a simplified representation of the system effectively reducing the dimensions of the Hessian matrix. In this representation the protein is broken into n_b blocks, each composed of one or more consecutive residues. The overall dynamic behavior is then described by the rigid-body (translational/rotational) motion of these blocks. In the original implementation of RTB,³² the all-atom Hessian matrix H is first computed explicitly. The block rotational-translational (T/R) matrix H_b is then obtained from H as:

$$H_b = P^T H P \quad (1)$$

where P is the so-called projection matrix and P^T is its transpose. The projection matrix is obtained by transforming the derivatives of potential function, V , in the atomic space to those in the block T/R space using the chain product, i.e.:

$$\frac{\partial V}{\partial X_{i,\alpha}} = \sum_{j=1,2,3} \sum \frac{\partial x_j}{\partial X_{i,\alpha}} \frac{\partial V}{\partial x_j} \quad \alpha = 1, 2, \dots, 6 \quad (2)$$

where the first sum is over all the atoms in block i ; $X_{i,\alpha}$ are the translational ($\alpha=1, 2, 3$) and rotational ($\alpha=4, 5, 6$) degrees of freedom for block i ; and x_j are the Cartesian coordinates.

Once the block T/R matrix H_b is constructed, the approximate low-frequency normal modes of the protein can be obtained by diagonalizing H_b . Since the size of matrix H_b , namely $6n_b \times 6n_b$, is greatly reduced when compared to that of the original all-atom Hessian matrix H , namely $3N \times 3N$, the RTB method can be employed to study much larger proteins than the standard NMA. Another advantage of the block-based method is that, due to the self-averaging effects within each block, the energy surface in block T/R space is smoother than that in atomic space. It has been shown that on a rugged energy surface with many local minima, the normal mode method, which expands the potential about a single local minimum, does not necessarily capture the desired transition from one minimum to another. Thus, the smoother energy surface resulting from the RTB model

should make it easier to observe large-scale conformational transitions.

It should be noted, however, in the RTB described above, the need for storing the full Hessian matrix at the first step somehow compromises the advantage of the method. In the current implementation in AMBER8[†], the block T/R Hessian matrix is constructed in a direct fashion. That is, once the second derivatives for each pair of atoms are calculated, they are directly projected onto the corresponding block Hessian elements. This idea has been pursued previously by Cui *et al.*,³¹ where “super blocks” were used to avoid the repetitive evaluation of the atomic second derivatives.

In our work, the main loop runs over each pair of atoms; for each pairwise interaction between atoms i and j , we first calculate its associated all-atom Hessian matrix elements, such as $\{(3(i-1)+\alpha, 3(i-1)+\beta), (3(i-1)+\alpha, 3(i-1)+\beta), (3(i-1)+\alpha, 3(j-1)+\beta), \alpha, \beta=1, 2, 3\}$. Each of the 36 atomic derivatives is then converted to block matrix elements according to the chain rule given in equation (2). It is worth noting that the interactions from any pair of atoms, which belong to the blocks I, J , respectively, only contribute to the corresponding matrix elements $\{(6(I-1)+i, 6(I-1)+j), (6(I-1)+i, 6(J-1)+j), (6(J-1)+i, 6(J-1)+j), i=1, 2, \dots, 6; j=1, 2, \dots, 6\}$ of the block T/R Hessian, while the interactions within the block contribute nothing to the block Hessian, thus can be neglected during the calculation. As the current implementation forgoes the need to store the large atomic Hessian matrix, it can be routinely used to study large proteins while still using a standard atomic potential. Compared to other more approximate methods such as the Gaussian network model⁴² and elastic network model,⁵⁴ the use of an all-atom potential should provide a more realistic description of the system, especially for highly charged or heterogeneous ones.

Equilibration and minimization

Before running NMA, the modeled structures were equilibrated with a 1 ns MD simulation with positional restraints on all C^α atoms. The equilibration utilized the generalized Born implicit solvent model⁵⁵ as implemented in AMBER8. The equilibrated structure was then subjected to three rounds of energy minimization. The system first underwent 500 steps of steepest descent minimization with restraints on all backbone atoms. This was followed by 5000 steps of conjugate-gradient minimization with steadily decreasing restraints on C^α atoms. The restraints were applied to prevent unrealistic perturbations from the initial structure. Finally, the structure was minimized for another 3000 steps with the conjugate-gradient algorithm and no restraints until a root-mean-square gradient of $\sim 0.01 \text{ kcal mol}^{-1} \text{ \AA}^{-1}$ was reached. The heavy-atom RMSDs of the final minimized structures for the models I and C were $\sim 1.1 \text{ \AA}$ and $\sim 1.6 \text{ \AA}$, respectively, from their corresponding starting structures. It should be noted that although the gradient threshold was much greater than that typically required for conventional NMA ($\sim 10^{-6} \text{ kcal mol}^{-1} \text{ \AA}^{-1}$), this gradient range was found to be sufficient for obtaining well-converged results with block-based NMA.³¹ The RTB calculations were performed with a modified AMBER8 program using the AMBER ff94 force field.⁵⁶ A distance-dependent dielectric ($1/4r$) was used with no cutoff for non-bonded interactions. All

calculations and analyses were performed on a Dell dual 2.0 GHz Pentium4 desktop machine with 2 GB of memory.

Root-mean-square fluctuations

The root-mean-square atomic fluctuations (RMSF) for the i th atom are given by⁵⁷:

$$\langle \Delta r_i^2 \rangle = \frac{k_B T}{m_i \omega_k} a_{ik}^2 \quad \text{for the } k\text{th normal mode} \quad (3)$$

$$\langle \Delta r_i^2 \rangle = \frac{k_B T}{m_i} \sum_{k=1}^{3N-6} \frac{a_{ik}^2}{\omega_k} \quad \text{for all the normal modes} \quad (4)$$

where m_i is the mass for atom i ; ω_k is the vibration frequency of mode k ; whilst a_{ik} is the i th component of the k th eigenvector.

Correlation analysis

The cross-correlation coefficient C_{ij} , between atoms i and j , is a measure of the correlated nature of their atomic fluctuations and is computed as follows:⁵⁷

$$\langle \Delta r_i \cdot \Delta r_j \rangle = \sum_{k=1}^{3N-6} \frac{k_B T}{\omega_k^2} \frac{a_{ik} a_{jk}}{\sqrt{m_i} \sqrt{m_j}} \quad (5)$$

$$C_{ij} = \langle \Delta r_i \cdot \Delta r_j \rangle / (\langle \Delta r_i \cdot \Delta r_i \rangle \langle \Delta r_j \cdot \Delta r_j \rangle)^{1/2} \quad (6)$$

the summation is over all $3N-6$ normal modes; m_i and m_j are the masses for atoms i and j ; ω_k is the vibration frequency of mode k ; whilst a_{ik} and a_{jk} are the i th and j th components of the k th eigenvector.

Comparison of normal modes

The overlap of two sets of normal modes a_i and a_j is defined by the inner product of the two modes as follows:⁵⁸

$$R_{ij} = \frac{a_i \cdot a_j}{|a_i| |a_j|} \quad (7)$$

The values of R_{ij} should range from -1 to 1 . A large R_{ij} value indicates that the two modes are highly similar.

Generating an open-channel model

Starting from the closed-channel structure¹⁰ (PDB code: 2BG9), 25 model structures were generated by displacing the initial structure along the two most dominant eigenvectors $\Delta R^{(1)}$ and $\Delta R^{(2)}$ obtained for model I. If the coordinates for the closed structure are represented by R_{close} , then the new set of the coordinates after displacement would be $R_{\text{new}} = R_{\text{close}} + y(x\Delta R^{(1)} + (1-x)\Delta R^{(2)})$, where x and y are two adjustable parameters that control the amplitude of the displacement. The process was repeated several times by varying the values of x and y . To ensure a smooth structure, the backbone RMSD was used as a restraint. If the new structure deviated more than 4 \AA from the closed structure, a reduced y would be used. Previously, an iterative procedure was used to ensure a small conformational change in each step.⁴⁷ However, in the current work a one-step treatment seemed sufficient to yield smooth structures. The generated structures were minimized within AMBER8. Of these, six structures had a backbone RMSD within 3 \AA of the closed structure and underwent pore-radius profile analysis with the aid of the

[†] <http://amber.scripps.edu>

HOLE program.⁵⁹ The reason for using a 3 Å threshold was that the gating movements were believed to be relatively small so as to preserve the energetically favored hydrophobic cores.

Acknowledgements

Support for this project was provided partly by NSF, NIH, SDSC, HHMI, NBCR and by the NSF Center for Theoretical Biological Physics. We thank Dr N. Unwin for providing us a low-resolution open channel structure.

Supplementary Data

Supplementary data associated with this article can be found, in the online version, at [doi:10.1016/j.jmb.2005.10.039](https://doi.org/10.1016/j.jmb.2005.10.039)

References

- Karlin, A. (2002). Emerging structure of the nicotinic acetylcholine receptors. *Nature Rev. Neurosci.* **3**, 102–114.
- Absalom, N. L., Lewis, T. M. & Schofield, P. R. (2004). Mechanisms of channel gating of the ligand-gated ion channel superfamily inferred from protein structure. *Expt. Physiol.* **89**, 145–153.
- Lester, H. A., Dibas, M. I., Dahan, D. S., Leite, J. F. & Dougherty, D. A. (2004). Cys-loop receptors: new twists and turns. *Trends Neurosci.* **27**, 329–336.
- Alberts, B., Johnson, A., Lewis, J., Raff, M., Roberts, K. & Walter, P. (2002). *Molecular Biology of the Cell*, 4th edit., Garland Publishing, New York.
- Grosman, C. & Auerbach, A. (2001). The dissociation of acetylcholine from open nicotinic receptor channels. *Proc. Natl Acad. Sci. USA*, **98**, 14102–14107.
- Brejč, K., van Dijk, W. J., Klaassen, R. V., Schuurmans, M., van Der Oost, J., Smit, A. B. & Sixma, T. K. (2001). Crystal structure of an ACh-binding protein reveals the ligand-binding domain of nicotinic receptors. *Nature*, **411**, 269–276.
- Celie, P. H., van Rossum-Fikkert, S. E., van Dijk, W. J., Brejč, K., Smit, A. B. & Sixma, T. K. (2004). Nicotine and carbamylcholine binding to nicotinic acetylcholine receptors as studied in AChBP crystal structures. *Neuron*, **41**, 907–914.
- Bourne, Y., Talley, T. T., Hansen, S. B., Taylor, P. & Marchot, P. (2005). Crystal structure of a Cbtx-AChBP complex reveals essential interactions between snake alpha-neurotoxins and nicotinic receptors. *EMBO J.* **24**, 1512–1522.
- Celie, P. H., Kasheverov, I. E., Mordvintsev, D. Y., Hogg, R. C., van Nierop, P., van Elk, R. *et al.* (2005). Crystal structure of nicotinic acetylcholine receptor homolog AChBP in complex with an alpha-conotoxin PnIA variant. *Nature Struct. Mol. Biol.* **12**, 582–588.
- Unwin, N. (2005). Refined structure of the nicotinic acetylcholine receptor at 4 Å resolution. *J. Mol. Biol.* **346**, 967–989.
- Unwin, N. (1995). Acetylcholine receptor channel imaged in the open state. *Nature*, **373**, 37–43.
- Horenstein, J., Wagner, D. A., Czajkowski, C. & Akabas, M. H. (2001). Protein mobility and GABA-induced conformational changes in GABA(A) receptor pore-lining M2 segment. *Nature Neurosci.* **4**, 477–485.
- Grosman, C., Salamone, F. N., Sine, S. M. & Auerbach, A. (2000). The extracellular linker of muscle acetylcholine receptor channels is a gating control element. *J. Gen. Physiol.* **116**, 327–340.
- Wang, H. L., Ohno, K., Milone, M., Brengman, J. M., Evoli, A., Batocchi, A. P. *et al.* (2000). Fundamental gating mechanism of nicotinic receptor channel revealed by mutation causing a congenital myasthenic syndrome. *J. Gen. Physiol.* **116**, 449–462.
- White, B. H. & Cohen, J. B. (1992). Agonist-induced changes in the structure of the acetylcholine receptor M2 regions revealed by photoincorporation of an uncharged nicotinic noncompetitive antagonist. *J. Biol. Chem.* **267**, 15770–15783.
- Hansen, S. B., Radic, Z., Talley, T. T., Molles, B. E., Deerinck, T., Tsigelny, I. & Taylor, P. (2002). Tryptophan fluorescence reveals conformational changes in the acetylcholine binding protein. *J. Biol. Chem.* **277**, 41299–41302.
- McCammon, J. A., Gelin, B. R. & Karplus, M. (1977). Dynamics of folded proteins. *Nature*, **267**, 585–590.
- Karplus, M. & McCammon, J. A. (2002). Molecular dynamics simulations of biomolecules. *Nature Struct. Biol.* **9**, 646–652.
- Henchman, R. H., Wang, H. L., Sine, S. M., Taylor, P. & McCammon, J. A. (2005). Ligand-induced conformational change in the {alpha}7 nicotinic receptor ligand binding domain. *Biophys. J.* **88**, 2564–2576.
- Law, R. J., Henchman, R. H. & McCammon, J. A. (2005). A gating mechanism proposed from a 15 nanosecond simulation of a complete human alpha7 nicotinic acetylcholine receptor model. *Proc. Natl Acad. Sci. USA*, **102**, 6813–6818.
- Schlitter, J., Engels, M., Kruger, P., Jacoby, E. & Wollmer, A. (1993). Targeted molecular dynamics simulation of conformational change—application to the T→R transition in insulin. *Mol. Sim.* **10**, 291–309.
- Isralewitz, B., Baudry, J., Gullingsrud, J., Kosztin, D. & Schulten, K. (2001). Steered molecular dynamics investigations of protein function. *J. Mol. Graph. Model.* **19**, 13–25.
- Kumar, S., Bouzida, D., Swendsen, R. H., Kollman, P. A. & Rosenberg, J. M. (1992). The weighted histogram analysis method (WHAM) for free energy calculations on biomolecules. 1. The method. *J. Comput. Chem.* **13**, 1011–1021.
- Jarzynski, C. (1997). Nonequilibrium equality for free energy differences. *Phys. Rev. Letters*, **78**, 2690–2693.
- Ma, J. & Karplus, M. (1998). The allosteric mechanism of the chaperonin GroEL: a dynamic analysis. *Proc. Natl Acad. Sci. USA*, **95**, 8502–8507.
- Xu, C., Tobi, D. & Bahar, I. (2003). Allosteric changes in protein structure computed by a simple mechanical model: hemoglobin T ↔ R2 transition. *J. Mol. Biol.* **333**, 153–168.
- Cui, Q., Li, G., Ma, J. & Karplus, M. (2004). A normal mode analysis of structural plasticity in the biomolecular motor F(1)-ATPase. *J. Mol. Biol.* **340**, 345–372.
- Tama, F., Valle, M., Frank, J. & Brooks, C. L., 3rd (2003). Dynamic reorganization of the functionally active ribosome explored by normal mode analysis and cryo-electron microscopy. *Proc. Natl Acad. Sci. USA*, **100**, 9319–9323.

29. Wang, Y., Rader, A. J., Bahar, I. & Jernigan, R. L. (2004). Global ribosome motions revealed with elastic network model. *J. Struct. Biol.* **147**, 302–314.
30. Zheng, W. & Brooks, B. (2005). Identification of dynamical correlations within the myosin motor domain by the normal mode analysis of an elastic network model. *J. Mol. Biol.* **346**, 745–759.
31. Li, G. & Cui, Q. (2002). A coarse-grained normal mode approach for macromolecules: an efficient implementation and application to Ca(2+)-ATPase. *Biophys. J.* **83**, 2457–2474.
32. Tama, F., Gadea, F. X., Marques, O. & Sanejouand, Y. H. (2000). Building-block approach for determining low-frequency normal modes of macromolecules. *Proteins: Struct. Funct. Genet.* **41**, 1–7.
33. Taly, A., Delarue, M., Grutter, T., Nilges, M., Le Novère, N., Corringer, P. J. & Changeux, J. P. (2005). Normal mode analysis suggests a quaternary twist model for the nicotinic receptor gating mechanism. *Biophys. J.* **88**, 3954–3965.
34. Grosman, C., Zhou, M. & Auerbach, A. (2000). Mapping the conformational wave of acetylcholine receptor channel gating. *Nature*, **403**, 773–776.
35. Labarca, C., Nowak, M. W., Zhang, H., Tang, L., Deshpande, P. & Lester, H. A. (1995). Channel gating governed symmetrically by conserved leucine residues in the M2 domain of nicotinic receptors. *Nature*, **376**, 514–516.
36. Kash, T. L., Jenkins, A., Kelley, J. C., Trudell, J. R. & Harrison, N. L. (2003). Coupling of agonist binding to channel gating in the GABA(A) receptor. *Nature*, **421**, 272–275.
37. Henchman, R. H., Wang, H. L., Sine, S. M., Taylor, P. & McCammon, J. A. (2003). Asymmetric structural motions of the homomeric alpha7 nicotinic receptor ligand binding domain revealed by molecular dynamics simulation. *Biophys. J.* **85**, 3007–3018.
38. Case, D. A. (1994). Normal mode analysis of protein dynamics. *Curr. Opin. Struct. Biol.* **4**, 285–290.
39. Gao, F., Bren, N., Burghardt, T. P., Hansen, S., Henchman, R. H., Taylor, P. *et al.* (2005). Agonist-mediated conformational changes in acetylcholine-binding protein revealed by simulation and intrinsic tryptophan fluorescence. *J. Biol. Chem.* **280**, 8443–8451.
40. Miyazawa, A., Fujiyoshi, Y. & Unwin, N. (2003). Structure and gating mechanism of the acetylcholine receptor pore. *Nature*, **423**, 949–955.
41. Unwin, N., Miyazawa, A., Li, J. & Fujiyoshi, Y. (2002). Activation of the nicotinic acetylcholine receptor involves a switch in conformation of the alpha subunits. *J. Mol. Biol.* **319**, 1165–1176.
42. Bahar, I., Atilgan, A. R. & Erman, B. (1997). Direct evaluation of thermal fluctuations in proteins using a single-parameter harmonic potential. *Fold. Des.* **2**, 173–181.
43. Hayward, S., Kitao, A. & Berendsen, H. J. C. (1997). Model-free methods of analyzing domain motions in proteins from simulation: a comparison of normal mode analysis and molecular dynamics simulation of lysozyme. *Proteins: Struct. Funct. Genet.* **27**, 425.
44. Xu, Y., Barrantes, F. J., Luo, X., Chen, K., Shen, J. & Jiang, H. (2005). Conformational dynamics of the nicotinic acetylcholine receptor channel: a 35-ns molecular dynamics simulation study. *J. Am. Chem. Soc.* **127**, 1291–1299.
45. Mitra, A., Bailey, T. D. & Auerbach, A. L. (2004). Structural dynamics of the M4 transmembrane segment during acetylcholine receptor gating. *Structure (Camb)*, **12**, 1909–1918.
46. Barrantes, F. J. (2003). Modulation of nicotinic acetylcholine receptor function through the outer and middle rings of transmembrane domains. *Curr. Opin. Drug Discov. Dev.* **6**, 620–632.
47. Miyashita, O., Onuchic, J. N. & Wolynes, P. G. (2003). Nonlinear elasticity, proteinquakes, and the energy landscapes of functional transitions in proteins. *Proc. Natl Acad. Sci. USA*, **100**, 12570–12575.
48. Dahan, D. S., Dibas, M. I., Petersson, E. J., Auyeung, V. C., Chanda, B., Bezanilla, F. *et al.* (2004). A fluorophore attached to nicotinic acetylcholine receptor beta M2 detects productive binding of agonist to the alpha delta site. *Proc. Natl Acad. Sci. USA*, **101**, 10195–10200.
49. Zhang, H. & Karlin, A. (1997). Identification of acetylcholine receptor channel-lining residues in the M1 segment of the beta-subunit. *Biochemistry*, **36**, 15856–15864.
50. Sali, A. & Blundell, T. L. (1993). Comparative protein modelling by satisfaction of spatial restraints. *J. Mol. Biol.* **234**, 779–815.
51. Sali, A., Potterton, L., Yuan, F., van Vlijmen, H. & Karplus, M. (1995). Evaluation of comparative protein modeling by MODELLER. *Proteins: Struct. Funct. Genet.* **23**, 318–326.
52. Laskowski, R. A., MacArthur, M. W., Moss, D. S. & Thornton, J. M. (1993). PROCHECK: a program to check the stereochemical quality of protein structures. *J. Appl. Crystallog.* **26**, 283–291.
53. Sippl, M. J. (1993). Recognition of errors in three-dimensional structures of proteins. *Proteins: Struct. Funct. Genet.* **17**, 355–362.
54. Tirion, M. M. (1996). Large amplitude elastic motions in proteins from a single-parameter, atomic analysis. *Phys. Rev. Letters*, **77**, 1905–1908.
55. Still, W. C., Tempczyk, A., Hawley, R. C. & Hendrickson, T. (1990). Semianalytical treatment of solvation for molecular mechanics and dynamics. *J. Am. Chem. Soc.* **112**, 6127–6129.
56. Cornell, W. D., Cieplak, P., Bayly, C. I., Gould, I. R., Merz, K. M., Ferguson, D. M. *et al.* (1995). A second generation force field for the simulation of proteins, nucleic acids, and organic molecules. *J. Am. Chem. Soc.* **117**, 5179–5197.
57. Brooks, C. L., 3rd, Karplus, M. & Pettitt, B. M. (1988). A theoretical perspective of dynamics, structure and thermodynamics. *Advan. Chem. Phys.* **71**, 1.
58. Tama, F. & Sanejouand, Y. H. (2001). Conformational change of proteins arising from normal mode calculations. *Protein Eng.* **14**, 1–6.
59. Smart, O. S., Neduvellil, J. G., Wang, X., Wallace, B. A. & Sansom, M. S. (1996). HOLE: a program for the analysis of the pore dimensions of ion channel structural models. *J. Mol. Graph.* **14**, 354–360.

Edited by G. von Heijne

(Received 12 September 2005; received in revised form 11 October 2005; accepted 12 October 2005)
Available online 8 November 2005